J Mater Sci (2007) 42:1279–1284
DOI 10.1007/s10853-006-1393-9

Evaluation of EB-PVD deposited Ni–Cr–Al alloy foil

Chunlong Guan · Guoqin Liu · Xiaodong He · Yingchun Shan

Received: 27 August 2004 / Accepted: 13 January 2006 / Published online: 25 January 2007

Abstract Ni–Cr–Al alloy foils were deposited at 900 °C from a target of Ni–Cr–Al alloy by EB-PVD, and then annealed at 760 °C in a high vacuum furnace for 16 h. Microstructure of as-deposited foil consisted of a large amount of fine grains with mean size of 90 nm. However, after annealing the grains grew obviously to an average size of 4 μm. In addition, long range chemical ordering of $L1_2$ type emerged in the annealed specimens, while no evidence of ordering structure were found in the deposited samples. The as-deposited foil exhibited a strong {111} texture on the evaporation side. Twin substructure was dominated within grains of as-deposited and annealed samples. The mechanical properties of the foils were examined using room tensile tests. The ultimate tensile strength of as-deposited and annealed samples is 780 and 767 MPa, respectively. Investigation of fracture surfaces from samples revealed that brittle fracture took place along boundaries of columnar crystals formed on the substrate side, while the equiaxed dimples were dominant on the evaporation side.

C. Guan (✉) · G. Liu
School of Materials Science and Engineering, Henan University of Technology, Henan 450007, P.R. China
e-mail: gcl_hit@163.com

X. He
Center for Composite Materials, Harbin Institute of Technology, Harbin 150001, P.R. China

Y. Shan
Dalian Maritime University, Dalian, China

Introduction

Recently, Ni–Cr–Al thin film coatings have been extensively studied due to their good mechanical properties and excellent high temperature oxidation resistance [1, 2]. They are attractive for application in microelectronics and as heat- and corrosion-resistant coating [3]. Electron beam physical vapor deposition (EB-PVD) provides a successful method for producing films, foils and coatings. For example, nano-scale microlaminated film and thermal barrier coatings of Yittria-stabilized Zirconia have been deposited by this process [4, 5]. Due to the transformation from a vapor to a solid film, metastable phases often form in as-deposited films. Eridon et al. [6] deposited Ni/Al multilayers using co-evaporation with ion-beam mixing, and found a number of metastable phases including an amorphous phase, a disordered crystalline phase and a hexagonal close-packed phase in the films. In addition, Banerjee and co-workers [7] studied on the microstructure of Ni–25Al thin film deposited on unheated substrate. The results of XRD and TEM indicated that as-deposited thin films consisted of an f.c.c. Ni(Al) phase, an h.p.c. Ni(Al)′ phase and a third Al-rich tetragonal phase.

The recent studies on Ni-based films mainly focus on their microstructure, but their mechanical properties were rarely reported in previous works, especially from the viewpoint of tensile properties. In this paper, a detailed characterization of the microstructure in EB-PVD deposited Ni–Cr–Al foils is reported. In addition, the mechanical properties of the foils from tensile test are investigated.

Experimental procedure

Ni–Cr–Al superalloy foil was prepared by EB-PVD. The chemical composition of Ni–Cr–Al ingot was prepared by vacuum melting Ni–22Cr–4Al–0.4Y (wt.%) alloy. The process of the preparation of superalloy foil by EB-PVD is shown in Fig. 1.

Prior to fabricating the superalloy foil, the resistance adhesive layer (CaF_2) with thickness of about 15 μm was deposited to prevent bonding between substrate and condensate. The Ni–Cr–Al ingots of 100 mm in diameter and 200 mm in length were filled in the a water-cooled crucible. A steel disk substrate with a diameter of 800 mm and 20 mm thickness was mounted on the vertical axis. The substrate was heated by electron beams and the temperature kept 900 °C. The vacuum was $5–6 \times 10^{-4}$ Pa during evaporation. The thickness of the superalloy foil could be controlled by adjusting the beam currents, the upward speed of the ingots and rotation speed of the substrate. The upward speed of the ingot and the rotation speed of the substrate were 0.16 mm/min and 36 rev/min, respectively. The deposition rate of the ingots was 1.8 μm/min. In this work, the Ni–Cr–Al superalloy foil with 0.2 mm thickness was prepared by EB-PVD, and then was separated from the substrate.

The surface of the tested alloy was ground to 1200-git and mechanically polished, and then etched with a solution of HCl, HNO_3, HF and H_2O. X-Ray diffraction experiment was conducted, using Cu Kα as the incident radiation. The foils were characterized using transmission electron microscopy (TEM). The TEM samples were electropolised with a solution of 7% perchloric acid and ethanol at –20~30 °C by a double jet electropoliser. The surface of the foil was examined by atomic force microscopy (AFM). The fracture surfaces were imaged using scanning electron microscopy (SEM). Tensile testing at room temperature was conducted at a loading rate of 5×10^{-4} s^{-1} by an Instron-5500.

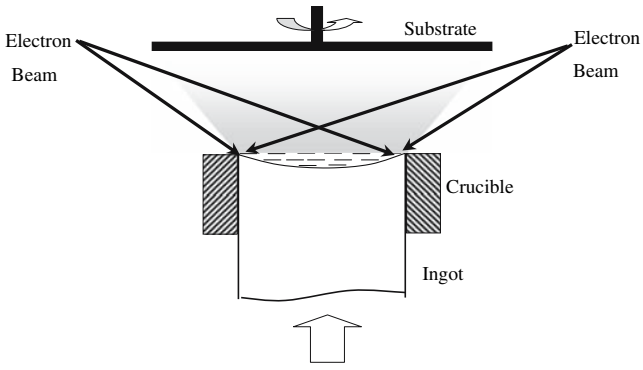

Fig. 1 Scheme of Ni–Cr–Al alloy foil deposition

Results and discussion

X-ray diffraction intensity patterns of both surface and evaporation side of Ni–Cr–Al foil deposited on a substrate temperature of 900 °C are shown in Fig. 2. The diffraction data from both surfaces of the foils and those of JCPDS card of Nickel are listed in Table 1. The presence of strong diffraction peaks indicates the formation of crystalline phases in this sample. The most intense diffraction from both surfaces adjacent to and away from the substrate occurred at $2\theta \approx 44°$,which corresponds to the interplanar spacing of 0.2058 and 0.2054 nm, respectively. In addition to the maximal intensity, several additional peaks are observed at $2\theta \approx 31°$, 51°, 75°, 91°and 97°, whose interplanar spacings are shown in Table 1. Except for

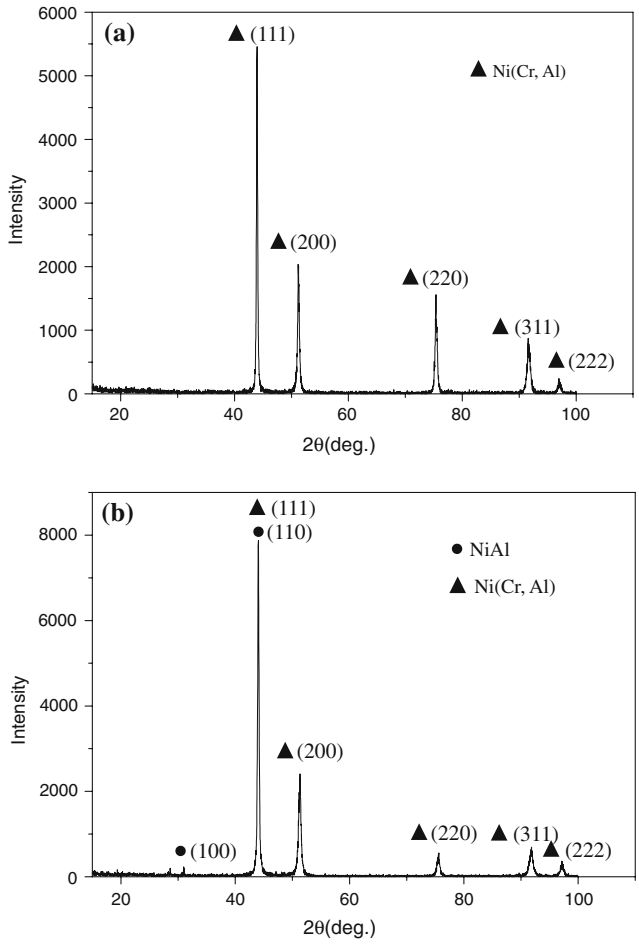

Fig. 2 XRD patterns of as-deposited Ni–Cr–Al foil from (**a**) the substrate and (**b**) the evaporation sides

Table 1 X-ray diffraction data of both surfaces of as-deposited Ni–Cr–Al alloy foil

Substrate side			Evaporation side		JCPDS card (040850)	
hkl	*d*/nm	*I*	*d*/nm	*I*	*d*/nm	*I*
(111)	2.0579	100	2.0544	100	2.0300	100
(200)	1.7813	38	1.7781	28	1.7600	42
(220)	1.2598	27	1.2570	6	1.2400	21
(311)	1.0742	15	1.0724	8	1.0600	20
(222)	1.0284	4	1.0270	4	1.0200	7

the peaks corresponding to $2\theta = 31.02°$, all peaks are in accordance with those of Ni element in the JCPDS card. Thus, the maximal intensity at $2\theta \approx 44°$can be indexed as the {111} peak of an f.c.c. Ni(Cr, Al) phase. The peak at $2\theta = 31.02°$ (see Fig. 2b) can be consistently indexed as the {100} peak of a cubic phase with a lattice parameter of $a = 0.2881$ nm, which is similar to the lattice parameter of NiAl phase. Lack of additional peaks makes it rather difficult to identify this phase solely based on XRD results. Compared to that of peaks in JCPDS card, the intensity of {200}, {220}, {311} peaks decreased significantly, which suggests that a strong {111} texture exhibited on the evaporation surface. However, no textures occurred on the substrate surface. Factors such as anisotropic surface energy, interface energy and elastic strain energy are primarily responsible for determining the preferred orientation in thin films [8]. The texture of PVD films is also influenced by the mobility of surface species on the growing film. Surface mobility can be influenced by substrate temperature, deposition rate, impurity adsorption, and use of energy-enhancement technology (i.e., electron, ion, or laser beam). The {111} crystalline texture is relative to the formation of columnar grains. Concurrent with growth of columnar grains is the evolution of crystallographic texture. The grains of the Ni–Cr–Al alloy films on the substrate side orient randomly, while microstructure on the evaporation side is oriented columnar grains. Initially, growth begins with the nucleation of randomly oriented grains on a likewise randomly oriented polycrystalline substrate. Continued growth produces a columnar film with an out-of-plane texture that increases in sharpness with increasing thickness. This result is well agreed with the reference [9]. In addition, the higher deposition rate is responsible for formation of texture on the evaporation side. Consequently, the preferred texture involves {111} planes with lower energy of the f.c.c. structure.

AFM image of Ni–Cr–Al foil is shown in Fig. 3a. The growth pattern of the foil is island-like. And in each ''island'' many fine columnar crystals, having constant angle with the orientation of the substrate normal, were observed. The average grain size is about 90 nm, and the roughness in this image ranges proximately from 100 to 600 nm. The SEM microghaph of the surface away from the substrate is shown in Fig. 3b. The morphology of the surface of as-deposited film is cauliflower-like, and each cauliflower consists of many fine grains. Through combined analysis of the images of AFM (see Fig. 3a) and SEM (see Fig. 3b) it is possible to attribute the fine grains in cauliflower cells to the columnar crystals in the ''island'' in Fig. 3a, and the cauliflowerr cells can be attribute to the ''island''. The microstructure of as-deposited Ni–Cr–Al foil is shown in the bright field micrograph from a plan-view TEM specimen in Fig. 4a. The inset in Fig. 4a is a plan-view selected area diffraction (SAD) pattern from the same specimen. The diffracted spots could be designated as nickel-based solution of f.c.c. phase with a

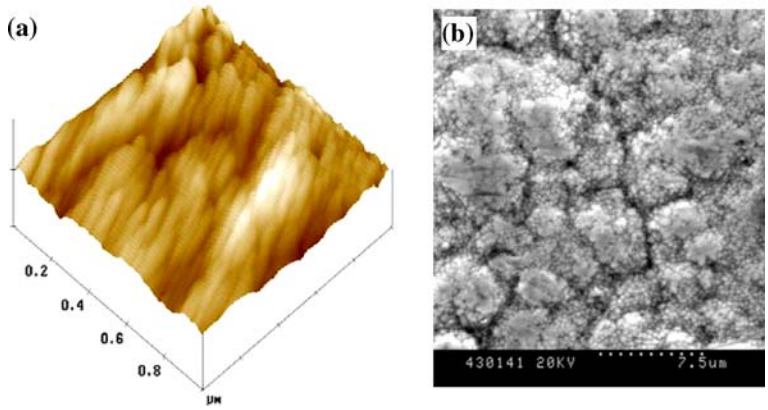

Fig. 3 Micrographs of the surface of as-deposited Ni–Cr–Al foil (**a**) AFM image (**b**) SEM image

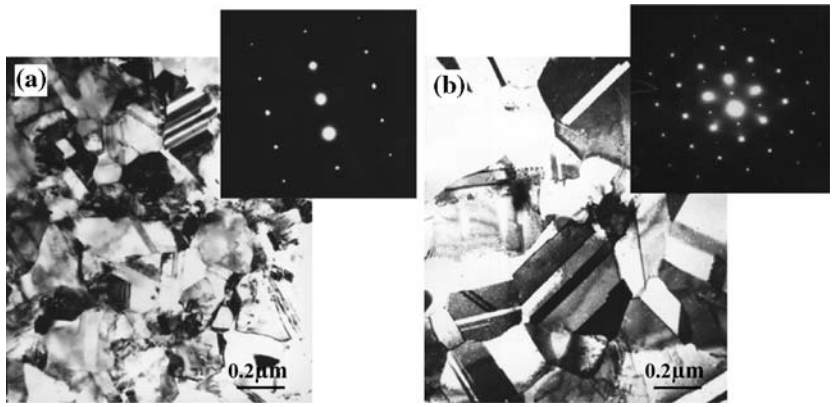

Fig. 4 (**a**) TEM micrograph showing the microstructure of as-deposited sample together with corresponding diffraction pattern in the inset. (**b**) TEM micrograph showing the microstructure of the sample after annealed at 760 °C for 16 h. A selected area diffraction pattern from the sample showing the ordering structure in the inset at the top right corner

lattice parameter of $a_{f.c.c} = 0.3600$ nm. However, the NiAl phase was not found in this specimen. Moreover, due to the lack of any superlattice spots there is no evidence that ordering phases formed. A high density of defects (twins) is visible within the grains, as shown in Fig. 4a. The TEM micrograph of annealed samples is shown in Fig. 4b. As shown in Fig. 4b, the grains in annealed samples grew obviously and the twins still dominated within grains. The presence of superlattice reflections indicates that long-range chemical ordering of the $L1_2$ type occurred, as shown in inset in Fig. 4b.

Room temperature tensile tests were performed on the as-deposited and annealed foils to determine their mechanical properties. The tensile stress–strain behaviors of as-deposited and annealed specimens are shown in Fig. 5. Test results indicated that the UTS of the deposited specimens was 780 MPa while that of the annealed specimens was 767 MPa. No evidence of yield point was seen in stress–strain curves from either of these specimens. The as-deposited condensates showed no sign of plastic deformation whereas the annealed deposits showed a ductile behavior. Some of earlier studies on investigations of mechanical properties of Ni–Cr–Al deposits were reported. In fact, rapid solidification processing of Ni-based alloys yields lower ductility in the as-deposited condition as compared to annealed [10–12]. SEM fractographs of fracture surfaces of as-deposited and annealed condesates are shown in Fig. 6. Figure 6a show the existence of two facture zones marked A and B. Zone A consisted of very shallow dimples indicating a large ductile component, as shown in Fig. 6b. A typical brittle fracture took place along boundaries of columnar crystals in zone B, as shown in Fig. 6c. Figure 7 presents fractographs of an annealed sample showing a much larger ductile region, a more pronounced neck, and deeper microvoids than Fig. 6a. The results of SEM fractures indicate that the ductility of annealed condensates is superior to that of as-deposited condensates. From the scanning electron micrographs of the fracture surfaces, it can be concluded that morphology of the grains on the evaporation side was columnar crystals while morphology of the grains on the substrate side was equiaxed crystals. The microstructure of deposited foil can be explained using the accepted physical vapor deposition zone models [13–16]. In all cases a widely accepted physical model tying the evolution of microstructure in PVD deposits to substrate temperature during deposition is the ''structure map'' first proposed by Movchan and Demchisin [16]. This model divides thick films into three unique microstructure ''zones'' based on the substrate temperature $T = T_s/T_m$ (normalized by the melting point of the evaporant, where T_s is substrate temperature, and T_m is the melting temperature of the condensate). Zone-I ($T < 0.3$) films are characterized by cone-shaped columns with rounded tops separated from one another by voided regions. Zone-II ($0.3 < T < 0.5$) microstructure consists of parallel, columnar grains with faceted tops. Finally, Zone-III ($T > 0.5$) may form in which the grains are no longer columnar but instead have equiaxed or equilibrium shapes. The deposited films

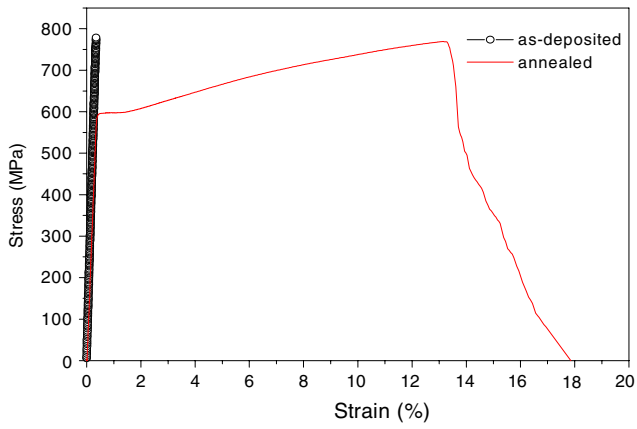

Fig. 5 Stress–strain behavior of as-deposited and annealed EB-PVD formed deposits

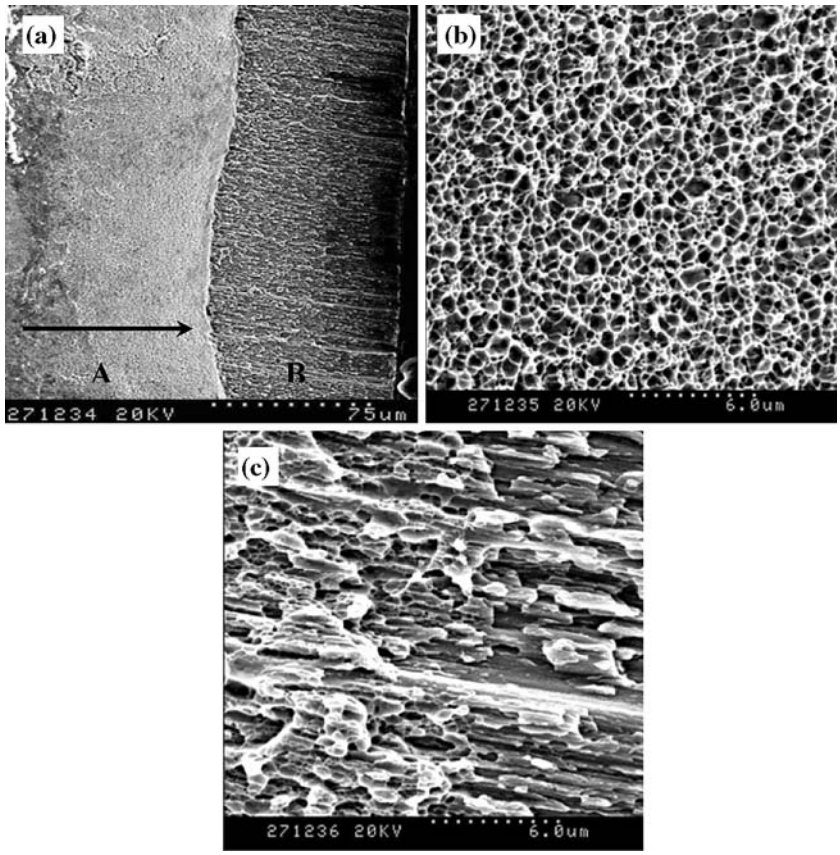

Fig. 6 SEM fractographs of fracture surfaces of as-deposited foil. (**a**) SEM fractograph showing the general fracture surface of the foil deposited at 900 °C. (**b**) High magnification SEM fractographs from zone A (ductile) and zone B (brittle) of the fracture surface shown in Fig. 7a. The arrow indicates the growth direction

in the present study exhibit features characteristic of Zone-III structure ($T \approx 0.6$) on the substrate side, which is agrees well with the above zone model, and Zone-II structure on the evaporation side.

Conclusions

Ni–Cr–Al alloy foils were deposited using EB-PVD method at 900 °C. Detailed microstructure, strength, and fracture behavior of as-deposited and annealed samples were characterized using X-ray diffraction, SEM and tensile testing. The results showed that the microstructure of alloy foils consisted of Zone-III grains (equiaxed grains) on the substrate side and Zone-II grains (parallel and columnar grains) on the evaporation side. As-deposited Ni–Cr–Al alloy foil exhibited a strong {111} texture on the evaporation side while no textures occurred on the substrate side, and had a fine-grained polycrystalline microstructure con-

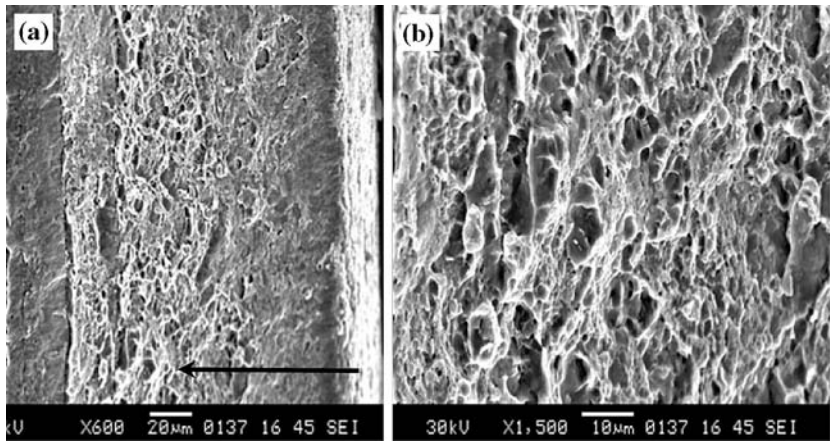

Fig. 7 SEM fractographs of fracture surfaces of annealed foil. (**a**) SEM fractograph showing the general fracture surface of the sample annealed at 760 °C for 16 h. (**b**) High magnification SEM fractograph from ductile zone of the fracture surface shown in Fig. 7a. The arrow indicates the growth direction

sisting of γ-Ni (Al) with a high density of twins. After annealing at 760 °C for 16 h long range ordering of $L1_2$ type presented in the samples. The EB-PVD processed Ni–Cr–Al foils showed rapid solidification such as fine grain size and high UTS values. The ductility of the deposits was relatively low but obviously improved after annealing at 760 °C for 16 h.

Acknowledgements The authors are grateful to the National Natural Science Foundation of China (Grant No. 50304007) that supported this research.

References

1. Chen GF, Lou HY (2000) Mater Lett 45:286
2. Wang B, Gong J, Wang AY et al (2002) Surf Coat Technol 149:70
3. Ohring M (1992) The materials science of thin films. Academic Press, Boston, MA, p 580
4. Rowe RG, Skelly DW, Larsen M (1994) Script Metal Mater 31:1487
5. Movchan BA (1996) JOM 11:40
6. Eridon JE, Was GS, Rehn LE (1988) J Mater Res 3(4):26
7. Banerjee R, Thompson GB, Anderson PM, Fraser HL (2003) Thin Solid Films 424:93
8. Shi Z, Craib GRG, Player MA, Tang CC (1997) Thin Solid Films 304:170
9. Schulz U, Schmucker M (2000) Mater Sci Eng A 276:1
10. Koch CC (1988) Int Met Rev 33:201
11. Choudhury A, White CL, Brooks CR (1986) Scr Metall 20:1061
12. Tiwari R, Sampath S, Gudmundsson B, Halada G et al (1995) Scr Metall 33:1159
13. Bunshah RF (1974) J Vac Sci Technol 11:633
14. Thornton JA (1977) Adv Rev Mater Sci 7:239
15. Grovenor CRM, Hentzelland HTG, Smith DA (1984) Acta Metall 32:773
16. Movchan BA, Demchishin AV (1969) Fiz Metal Metalloved 28:653